

# Effects of GDNF-Loaded Injectable Gelatin-Based Hydrogels on Endogenous Neural Progenitor Cell Migration

Deniece Fon, Aswan Al-Abboodi, Peggy P. Y. Chan, Kun Zhou, Peter Crack, David I. Finkelstein, and John S. Forsythe\*

Brain repair following disease and injury is very limited due to difficulties in recruiting and mobilizing stem cells towards the lesion. More importantly, there is a lack of structural and trophic support to maintain viability of the limited stem/progenitor cells present. This study investigates the effectiveness of an injectable gelatin-based hydrogel in attracting neural progenitor cells (NPCs) from the subventricular zone (SVZ) towards the implant. Glial cell-line-derived neurotrophic factor (GDNF) encapsulated within the hydrogel and porosity within the hydrogel prevents glial scar formation. By directly targeting the hydrogel implant towards the SVZ, neuroblasts can actively migrate towards and along the implant tract. Significantly more doublecortin (DCX)-positive neuroblasts surround implants at 7 d post-implantation (dpi) compared with lesion alone controls, an effect that is enhanced when GDNF is incorporated into the hydrogels. Neuroblasts are not observed at the implant boundary at 21 dpi, indicating that neuroblast migration has halted, and neuroblasts have either matured or have not survived. The development of an injectable gelatin-based hydrogel has significant implications for the treatment of some neurodegenerative diseases and brain injuries. The ability of GDNF and porosity to effectively prevent glial scar formation will allow better integration and interaction between the implant and surrounding neural tissue.

## 1. Introduction

The prognosis for the complete recovery of neurological function after acute neural injury or degenerative brain disease is poor. The endogenous regenerative capacity is dampened by the following: 1) neurons are post-mitotic and, therefore, are not easily replaced;<sup>[1]</sup> 2) neuroinflammation within the brain creates an environment that is not conducive for neural regeneration.<sup>[2]</sup> Current clinical treatments targeting acute neural injuries such as traumatic brain injury (TBI) are centered on controlling intracranial pressure in an attempt to preserve the surviving tissue. Currently, there is no effective treatment that reduces secondary cell death resulting from blood–brain barrier breakdown, dampens inflammation, and allows the brain to remodel after injury.<sup>[3–5]</sup> However, there is increasing pre-clinical evidence for the existence of defined cellular processes that, if stimulated, may have some promise in rebuilding the damaged part of the brain after TBI.<sup>[6]</sup>

Regeneration of damaged tissue is often hampered by the inhibitory extracellular environment in the adult brain (e.g., myelin basic protein that reduces axonal elongation). Recently, research focus has been directed towards harnessing the potential of neural stem/progenitor cells. Neural stem/progenitor cells exist in highly localized niches and are often difficult to mobilize to the site of damage where they are required. Delivery of exogenously derived stem cells is one approach to supplying stem cells directly where they are required. Currently, the most pertinent issues in exogenous stem cell delivery pertain to the source of cells; ethical issues for embryonic stem cells; and the intensive labor required in obtaining sufficiently large populations of adult stem cells for therapeutic use, in addition to possible tumorigenic and immune response upon engraftment.<sup>[7]</sup> Therefore, efforts to assist regeneration in the brain would benefit greatly if endogenous populations of stem cells can be harnessed as a source of cell replacement, bypassing the need of exogenous stem cell delivery.

Two stem cell niches have been identified in the adult brain, which exist in the subgranular zone (SGZ) within the hippocampus, and the subventricular zone (SVZ). Various injury/disease models in rodents, including models of stroke

D. Fon, Dr. K. Zhou, Dr. J. S. Forsythe  
Department of Materials Engineering  
Monash University  
Clayton, VIC, 3800, Australia  
E-mail: john.forsythe@monash.edu

A. Al-Abboodi  
Department of Chemical Engineering  
Monash University  
Clayton, VIC, 3800, Australia

A. Al-Abboodi, Dr. P. P. Y. Chan  
Micro/Nanophysics Research Laboratory  
RMIT University  
Melbourne, VIC, 3000, Australia

Dr. P. P. Y. Chan  
Melbourne Centre for Nanofabrication  
Clayton, VIC, 3168, Australia

Dr. P. Crack  
Department of Pharmacology  
The University of Melbourne  
Parkville, VIC, 3010, Australia

Dr. D. I. Finkelstein  
Florey Institute of Neuroscience and Mental Health, Parkville  
The University of Melbourne  
VIC, 3010, Australia

DOI: 10.1002/adhm.201300287



and penetrating brain injury, have demonstrated the migration of stem/progenitor cells from the SVZ towards large lesions, where they can differentiate into neuronal phenotypes appropriate to the anatomical location.<sup>[8–10]</sup> Utilization of these migrating stem cells for regenerative purposes is limited by poor survival rates,<sup>[8]</sup> which is likely due to the absence of appropriate structural and trophic support at the site of lesion. In this context, implantation of a hydrogel can potentially increase the viability of endogenously derived stem cells through structural support and presentation of a more permissive microenvironment. Moreover, presence of appropriate growth factors within the implant site can prove crucial for long-term survival of neural progenitor cells (NPCs). This provides a strong incentive for the incorporation of growth factors into hydrogel implants. Glial cell-line-derived neurotrophic factor (GDNF) is commonly used in neural tissue engineering because of its implications as a survival factor in many neurodegenerative disease and stroke models.<sup>[11,12]</sup> GDNF has potent survival effects on midbrain dopaminergic and other neurons,<sup>[13–15]</sup> hence it has therapeutic potential in Parkinson's disease. In addition, GDNF administration following experimental models of stroke has neuroprotective effects by significantly reducing lesion size.<sup>[11]</sup> Therefore, it is hypothesized that a reduction in inflammation and increased NPC survival can be achieved through the incorporation of GDNF into gelatin-based hydrogel implants.

Gelatin is a derivative of collagen, which is obtained by controlled thermal denaturation and hydrolysis of intermolecular amide bonds.<sup>[16]</sup> Collagen is a structural protein that is a major constituent in the extracellular matrix (ECM) of most connective tissues, though it is not present in the brain.<sup>[17]</sup> Collagen- and gelatin-based biomaterials are commonly used in many tissue engineering applications (including bone, cartilage, blood vessel, among others) due to their proven biocompatibility and general ability to improve cell attachment, thus increasing cell–biomaterial interaction.<sup>[18–20]</sup> Gelatins' utility as a scaffold in the brain has not been extensively studied. Due to current limitations to the fabrication methods of collagen- and gelatin-based hydrogels, these implants must be preformed prior to surgery.<sup>[10,21,22]</sup> Consequently, their uses as implants are limited to injury models pertaining to large lesions within the brain, often targeted to superficial structures such as the cerebral cortex, or extensive damage including deeper brain structures through penetrating ballistic-like brain injury (PBBi). Therefore, the effectiveness of gelatin-based, injectable hydrogels in assisting regeneration in the brain would benefit from a less invasive method of implantation.

An injectable, *in situ* forming, gelatin–hydroxyphenylpropionic acid (Gtn–HPA) hydrogel has the potential to reconstruct a neural pathway, and also has the capability of independent tuning of gelation rate and gel stiffness.<sup>[23]</sup> Through variations in concentrations of gelatin, horseradish peroxidase (HRP), and dilute H<sub>2</sub>O<sub>2</sub> (catalyst and oxidant, respectively), gel stiffness ranging from 280 Pa to 12.8 kPa, and gelation time ranging from seconds to 25 min can be achieved. The ability to control gel stiffness allows the hydrogel to mimic the physical properties of the brain; while the ability to achieve gelation times in the order of minutes is of practical importance in allowing sufficient handling time during surgery. The biocompatibility of

Gtn–HPA has been demonstrated in previous *in vitro* studies with neural stem cells and mesenchymal stem cells, in which over 90% of cell viabilities were obtained.<sup>[23–26]</sup> The hydrogel can also support cell survival, proliferation, migration through the gel, and differentiation of hMSCs into the neuronal lineage.<sup>[23]</sup> Gelatin hydrogels are susceptible to hydrolysis of amide bonds; however, biodegradation is likely to be dominated enzymatically by various proteases secreted by cells, most prominent of which are the matrix metalloproteases (MMPs) MMP-2 and MMP-9 (also known as gelatinase-A and gelatinase-B, respectively).<sup>[16]</sup> Cellular secretions of these proteases are likely to enable encapsulated cells to migrate through the hydrogel *in vitro* through degradation of surrounding gelatin matrix. However, the lack of intrinsic macropores within Gtn–HPA can act as a barrier to cellular infiltration *in vivo*. Hence, a porous injectable Gtn–HPA hydrogel was previously developed by our group, and was employed as a cell-supporting substrate for 3D imaging.<sup>[27]</sup> In this system, a second HRP-crosslinkable polymer, carboxymethylcellulose (CMC) conjugated to tyramine (Tyr; CMC–Tyr), was introduced in Gtn–HPA solution; the same HRP-catalyzed crosslinking mechanism was utilized, but phase separation occurred during gelation to give rise to pore formation within the hydrogel. For brevity, the hydrogel composed of Gtn–HPA only is denoted as *Gtn*, and the porous hydrogel composed of Gtn–HPA and CMC–Tyr is denoted as *pGtn*.

The utilization of *in situ*-forming hydrogels as brain implants to assist neural regeneration has been limited but includes xyloglucan<sup>[28]</sup> and self-assembling copolypeptide<sup>[29]</sup> hydrogels. Gel formation in both these materials occurs via physical interactions between polymer components, in particular, through hydrophobic interactions, as opposed to chemical crosslinking. When implanted into rat brains, poly-D-lysine (PDL)-functionalized xyloglucan-supported cellular infiltration from the surrounding parenchyma, including astrocytes and neurites.<sup>[28]</sup> However, the versatility of this material is limited because mechanical properties of the gel are not readily tunable, and xyloglucan is not enzymatically degradable within the brain. On the other hand, self-assembling copolypeptide hydrogels are highly versatile because various properties can be readily and independently tuned through gel composition.<sup>[29]</sup> Although implantation of these materials into mouse brains supported abundant cell ingrowth, it was unable to attract neurite infiltration. In this respect, Gtn–HPA hydrogels are candidate materials for brain repair applications because it allows independent tuning of mechanical properties and gelation rate, it is biodegradable, and can support cell growth *in vitro*.

This study investigated the effectiveness of an injectable gelatin-based hydrogel in attracting NPC migration from the SVZ, and its ability to support NPC survival. GDNF was encapsulated into the hydrogel as a means of growth factor delivery to reduce reactive gliosis, support NPC survival, and infiltration into the hydrogel. The injection of the hydrogel aims to minimize tissue damage that is otherwise unavoidable for implantation of preformed scaffolds. A novel strategy employed in this study was to implant the hydrogel such that it directly intercepts the source of NPCs (i.e., the SVZ and rostral migratory stream, RMS) in order to directly and more efficiently attract NPCs to the implant.

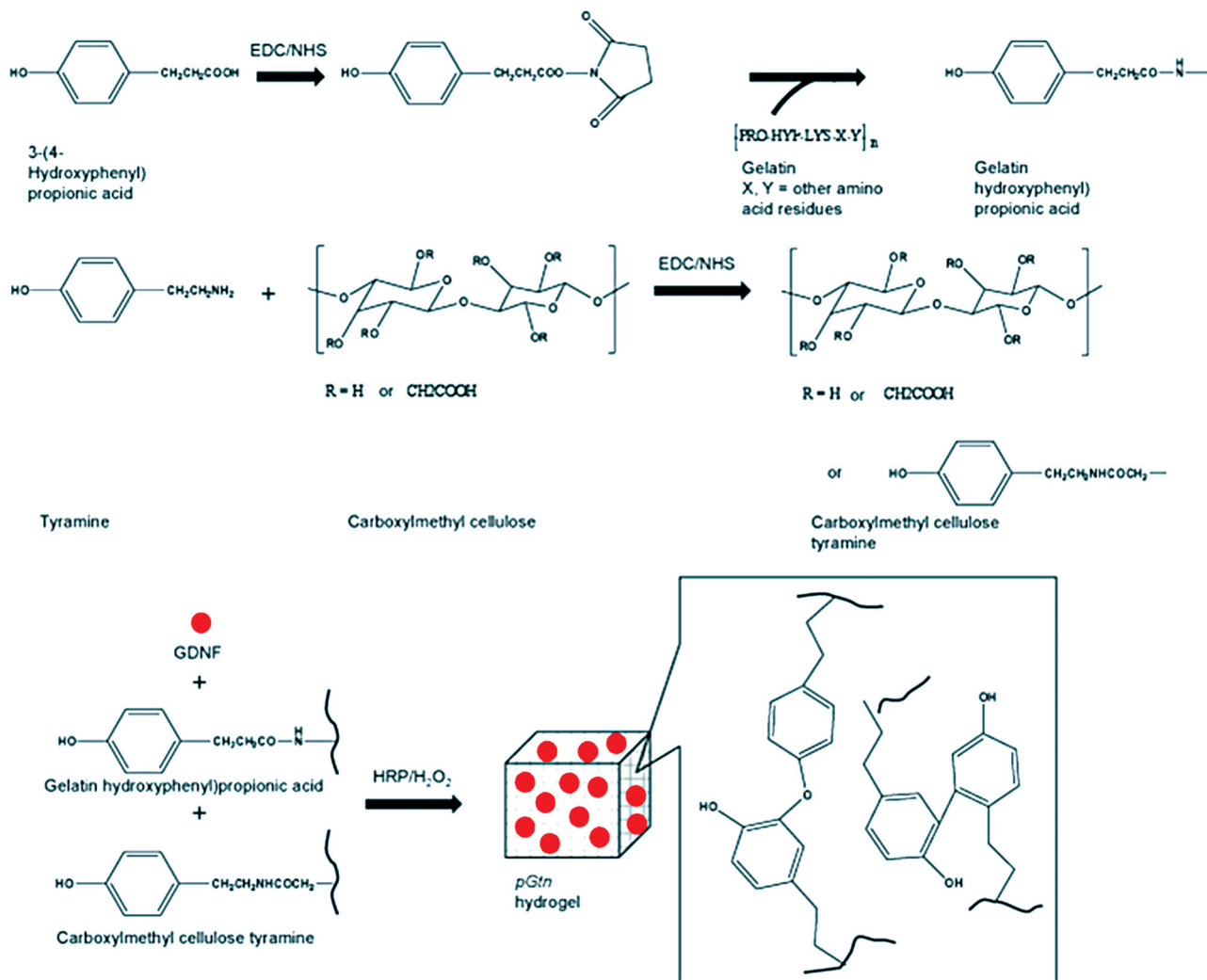


**Figure 1.** Schematic of the synthesis of Gtn-HPA and CMC-Tyr conjugates, and the subsequent encapsulation of GDNF during hydrogel formation.

## 2. Results

### 2.1. Hydrogel Characterization

Gtn-HPA and CMC-Tyr conjugates were synthesized via a general carbodiimide/active ester-mediated coupling reaction. These conjugates were mixed and crosslinked by HRP with dilute H<sub>2</sub>O<sub>2</sub> as oxidant to form an in situ hydrogel according to **Figure 1**. The swelling ratios of *pGtn* hydrogel formed from different HRP concentrations are provided in Figure S1 (Supporting Information). The swelling ratios were found to decrease with increasing HRP concentration, which can be attributed to the decrease in hydrogel porosity (to be described in later section).

Representative confocal microscopy images in **Figure 2** show the morphology of hydrated *pGtn* hydrogels, revealing its interconnected porous structure. This type of porous structure was also evident in scanning electron microscopy (SEM) images (Figure 2) of lyophilized *pGtn* hydrogels. The pore size of *pGtn*

hydrogel decreased with increasing HRP concentration. The wall of the hydrated hydrogel is much thicker than that of the lyophilized hydrogel due to the uptake of water, giving rise to smaller pore size in the hydrated structure.

The pore size and porosity of lyophilized *pGtn* hydrogels were further characterized by mercury porosimetry (Table S1, Supporting Information). The *pGtn* hydrogel exhibited pore size and porosity ranging from 18 to 52  $\mu\text{m}$  and 31–86%, respectively. Pore size and porosity decreased with increasing HRP concentration and was consistent with the trend observed under SEM.

### 2.2. Astrocyte Response

Following an injury to brain tissue, astrocytes become activated as part of a concerted response to protect the intact tissue partly via demarcation from necrotic tissue.<sup>[30]</sup> One of the hallmarks of reactive astrocytes is the upregulation of GFAP. GFAP

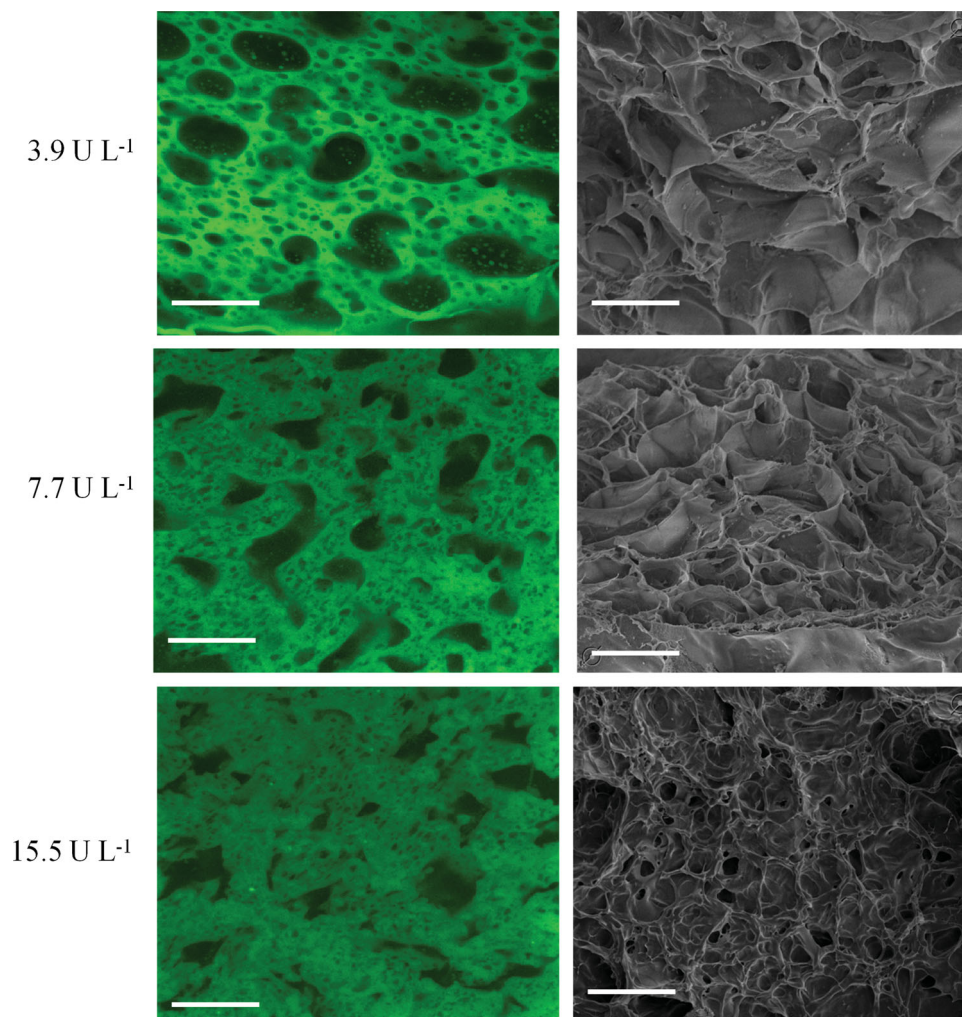


**Figure 2.** Confocal microscopy (left) and SEM (right) images showing pore size and morphology of swollen *pGtn* hydrogel and lyophilized *pGtn* hydrogel, respectively. The *pGtn* hydrogels were produced using different concentrations of HRP (3.9, 7.7, and 15.5 U L<sup>-1</sup>) and diluted H<sub>2</sub>O<sub>2</sub> ( $49.8 \times 10^{-6}$  M). Scale bar = 20  $\mu$ m.

expression was quantified by measuring fluorescence intensity relative to an equivalent uninjured region of the brain.

In terms of GFAP expression as a function of time and distance away from the site of implant, *Gtn* elicited the same response compared to injury alone (Figures 3, 4). This was characterized by intense GFAP expression immediately adjacent to the implant (within 200  $\mu$ m) at 7 d post-implantation (dpi) [injury:  $3.52 \pm 0.14$ ; *Gtn*:  $3.25 \pm 0.11$ ]. In contrast, the level of GFAP expression within 400  $\mu$ m of the edge of the implant was significantly lower ( $p < 0.05$ ) for all other implant conditions at both 7 and 21 dpi [7 dpi: *pGtn* =  $2.79 \pm 0.11$ , *Gtn+GDNF* =  $2.65 \pm 0.09$ , *pGtn+GDNF* =  $2.57 \pm 0.07$ ; 21 dpi: *pGtn* =  $1.35 \pm 0.06$ , *Gtn+GDNF* =  $1.58 \pm 0.03$ , *pGtn+GDNF* =  $1.43 \pm 0.05$ ] compared to *Gtn* and injury only. Interestingly, there was no significant difference in the GFAP expression profile between the implant conditions *pGtn*, *Gtn+GDNF*, and *pGtn+GDNF* (Figure 4).

For all implant conditions, GFAP expression was drastically elevated at 7 dpi but had partially subsided by 21 dpi, which is typical of the astrocytic response to a stab wound

injury.<sup>[31]</sup> However, the reduction in GFAP expression within 200  $\mu$ m of implant edge was greater for *pGtn*, *Gtn+GDNF*, and *pGtn+GDNF* (52%, 40%, and 44% reduction from 7 to 21 dpi, respectively), and more significantly, GFAP expression had returned to levels that were equivalent to that of the uninjured brain much closer to the edge of implant, compared with injury and *Gtn* (32% and 25% reduction, respectively).

Cellular hypertrophy and GFAP upregulation are typical characteristics of reactive astrocytes. Despite the similarities in GFAP expression, there were differences in morphology of reactive astrocytes between injury and *Gtn* conditions. Following injury, GFAP+ cells within 100  $\mu$ m of the lesion boundary extend thick processes that are highly oriented perpendicular to the lesion boundary. At the lesion boundary, the processes of reactive astrocytes extend parallel to the lesion boundary, forming a physical barrier that manifests itself as the glial scar. Implants of *Gtn* only exhibit similar morphology to the extent that reactive astrocytes extend processes parallel to the implant-tissue interface, however, the highly directed process extension towards the

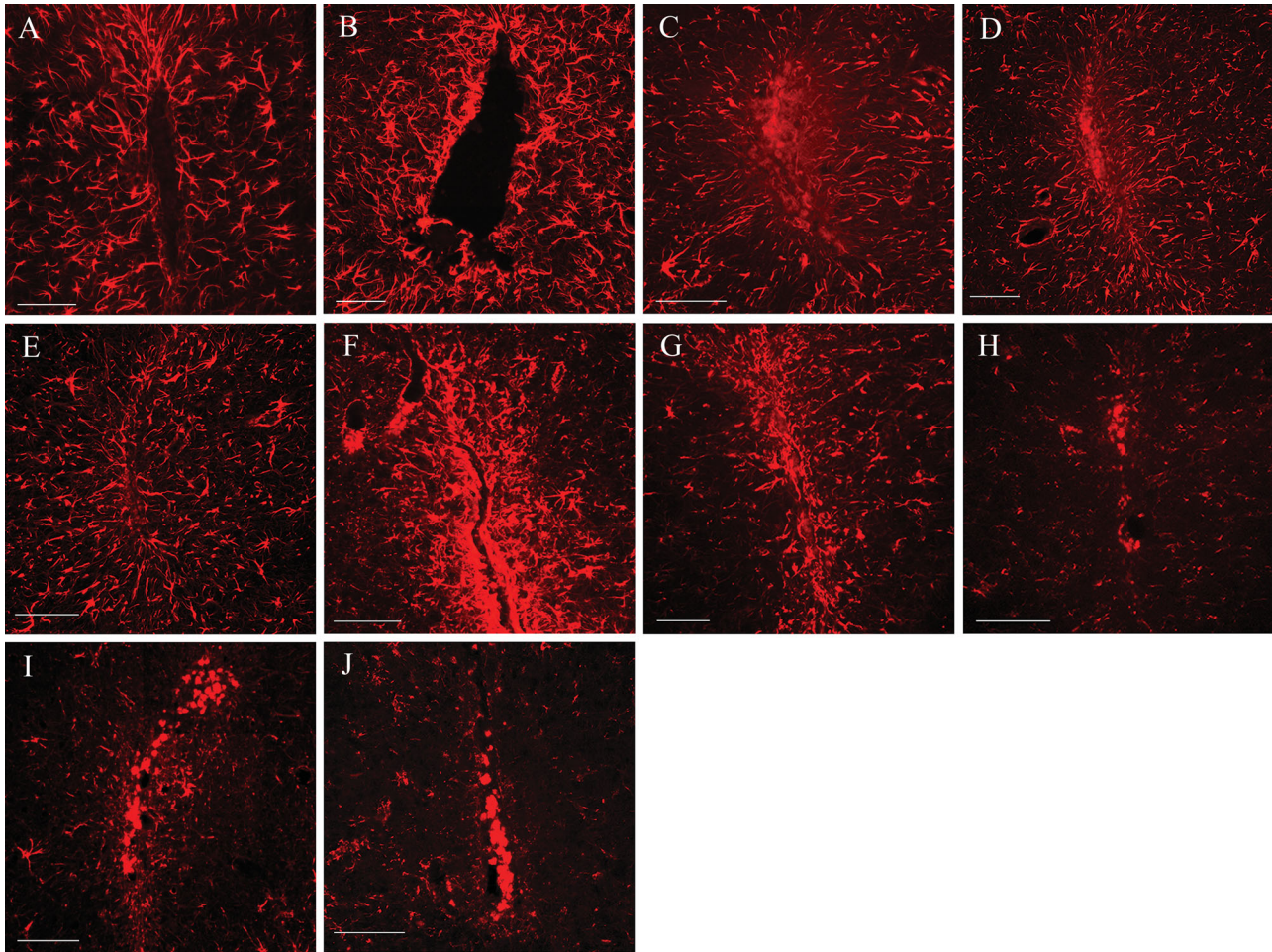


**Figure 3.** Representative images of horizontal tissue sections immunohistochemically stained for GFAP. Reactive astrocytes surrounding implant/lesion at 7 dpi (A–E) and 21 dpi (F–J). Injury (A,F), *Gtn* (B,G), *pGtn* (C,H), *Gtn+GDNF* (D,I), *pGtn+GDNF* (E,J). Scale bar = 100  $\mu\text{m}$ .

implant was generally not observed, where process outgrowth appeared randomly oriented (Figure S2, Supporting Information). For all other implant conditions, there was streaming of astrocytic processes towards the implant, but these processes very rarely extend parallel to the implant-tissue boundary. There was minimal astrocyte infiltration of *pGtn*. In contrast, GDNF induced a greater degree of infiltration; however, the extent was variable and may be partially determined by the local lesion size, where greater infiltration can be seen for small lesions. By 21 dpi, reactive astrocytes appear to have completely occupied the lesion as a glial scar in the injury group, and a mild glial scar persisted around *Gtn* hydrogel implants. For other implant conditions, no glial scar was evident, and astrocyte infiltration was variable, presumably due to hydrogel degradation.

### 2.3. Distribution of Doublecortin-Positive Neuroblasts in Response to Hydrogel Implant

Doublecortin (DCX) is a protein that is expressed transiently in immature and migrating neuroblasts. DCX+ cells were

observed surrounding all implants (*Gtn*, *Gtn+GDNF*, *pGtn*, and *pGtn+GDNF*) at 7 dpi, but only to a much smaller extent in animals subjected to injury only (Figure 5). Even when the injury directly impinged onto the SVZ, no DCX+ cells were observed within the lesion core. Whereas under implant conditions, DCX+ cells were mostly located at the implant-tissue interface, and only very occasionally within the implant; however, this was difficult to quantify due to dislodgement of the implant during tissue processing. Migrating DCX+ cells between the SVZ and the implant were only occasionally observed 7 dpi, and were not present 21 dpi. Some DCX+ cells appear to migrate towards the implant along the horizontal plane via the brain parenchyma, while others migrate along the length of the implant tract in the dorsal-ventral axis (Figure 6). DCX+ cell migration along the external surface of the implant tract can occur up to the level of the cortex. The distribution of DCX+ cells along the implant tract was neither uniform nor continuous. When considering the length of the implant tract, the amount of DCX-immunoreactivity decreased with increasing distance from the SVZ, but there was a distinct increase in DCX+ cells when the implant traversed the midline of the brain (when implant was crossing

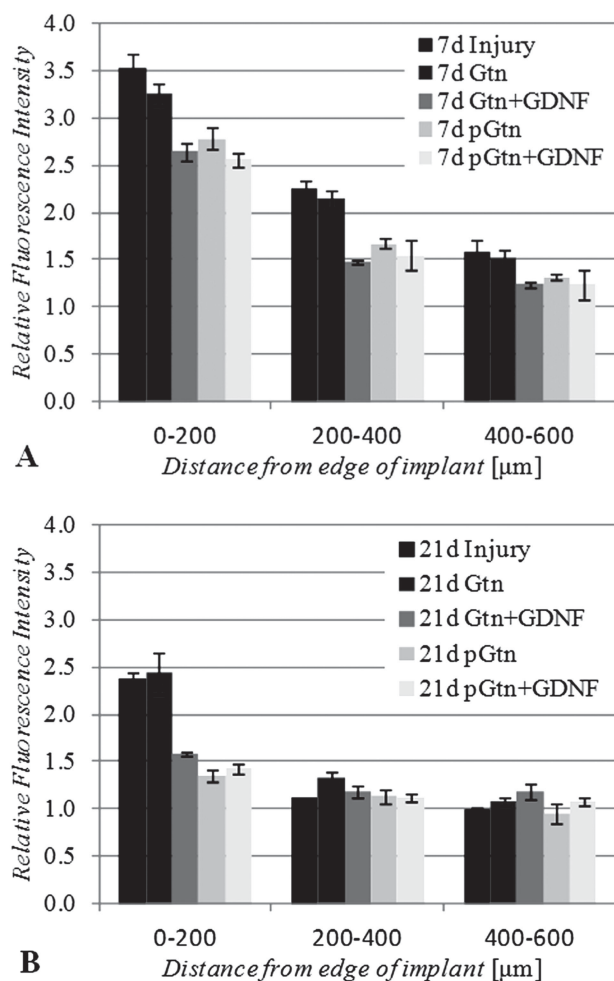


**Figure 4.** Profile of astrocyte activation, measured as GFAP fluorescence intensity relative to the non-injured part of the brain, as a function of distance from the edge of implant/injury for different implant conditions at A) 7 dpi, and B) 21 dpi. A) At 7 dpi, the GFAP fluorescence intensity for *Gtn+GDNF*, *pGtn*, and *pGtn+GDNF* were all significantly lower ( $p < 0.05$ ) than injury and *Gtn* at both 0–200 and 200–400  $\mu\text{m}$ . B) At 21 dpi, GFAP fluorescence intensity for *Gtn+GDNF*, *pGtn*, and *pGtn+GDNF* were all significantly lower ( $p < 0.001$ ) than injury and *Gtn* at 0–200  $\mu\text{m}$  only.

from the left hemisphere to the right) (Figure S3, Supporting Information). Assuming DCX+ cells migrated along the length of the implant, this represents a migration distance of up to 2.5 mm from the SVZ to the midline of the brain, along the dorsal–ventral direction. DCX+ cells were not observed outside the SVZ at 21 dpi for all treatment groups.

When GDNF was incorporated into the hydrogel, there was greater DCX+ staining surrounding the hydrogel. GDNF incorporation led to more DCX+ processes at greater distances from the implant surface. In addition, DCX+ cells surrounding *Gtn* and *pGtn* implants exhibited shorter processes and a more stellate cellular morphology compared with their GDNF counterparts, where DCX+ cells had longer processes and a more polarized morphology that is indicative of migratory behavior. This suggests that GDNF delivery may have acted as an additional

source of signaling and sustained neuroblast migration for a longer period of time. However, no DCX+ cells were observed surrounding implants with GDNF, indicating that the amount of GDNF delivered was insufficient to maintain long-term neuroblast migration.

The only exception to this pattern of DCX+ cell distribution occurred in the presence of unexpectedly large lesions (>1 mm diameter), in which case, DCX+ cells were observed both migrating towards, and located at the lesion boundary, at both 7 and 21 dpi (Figure 7). Similar to neuroblast migration observed in *Gtn*-based implants, neuroblasts from the SVZ migrated dorsally along the injury tract towards more dorsal regions of the brain, up to the level of the cortex. These occurrences were considered outliers (such large lesions occurred only four times across all treatment groups,  $n = 80$  injections), where the large injury was likely the result of excessive bleeding during surgery.

#### 2.4. Neurite Sprouting in Response to Hydrogel Implant

SMI32+ staining was most prevalent at 7 dpi, for all implant conditions as well as injury only. Neurite sprouting is most prominent within 100  $\mu\text{m}$  of lesion, but it does not extend into the lesion in injury only animals. In all implant conditions, there was a certain degree of interaction between neurites and material (Figure 8). However, in the presence of GDNF, there was more axonal regeneration at the implant interface, as well as a greater degree of neurite infiltration into the implant. This may reflect the increased interactions between neurites bridging the defect from opposite ends of the hydrogel. However, similar to DCX staining, SMI32+ staining reduced significantly at 21 dpi, with no enhanced neurite sprouting in the vicinity of the implant or lesion.

### 3. Discussion

#### 3.1. Synthesis and Characterization of Hydrogel

Swelling ratio is a measure of wettability, and high wettability is considered advantageous for tissue engineering and protein delivery applications because such aqueous environments can prevent denaturation of delicate proteins. A material with high wettability is also highly permeable, facilitating mass transport of oxygen, nutrient, and metabolites.<sup>[23,32]</sup> *pGtn* hydrogels exhibited high swelling ratio, which is desirable for preventing protein denaturation.

The pore size and interconnected porosity of hydrogels play an important role in regulating tissue regeneration. A substantial amount of porosity is necessary in enabling certain critical cellular events to occur, including cell binding, cell migration, ECM deposition, and vascularization.<sup>[33,34]</sup> Although porous scaffolds can be fabricated via numerous methods, including particulate leaching, gas forming, electrospinning, emulsion freeze-drying, fiber bonding, and photopatterning,<sup>[35]</sup> the majority of these techniques are not suitable for fabrication of in situ hydrogels. In this study, a porous hydrogel was fabricated using phase separation approach; due to the differences in hydrophobicity/hydrophilicity of *Gtn*–HPA and CMC–Tyr,

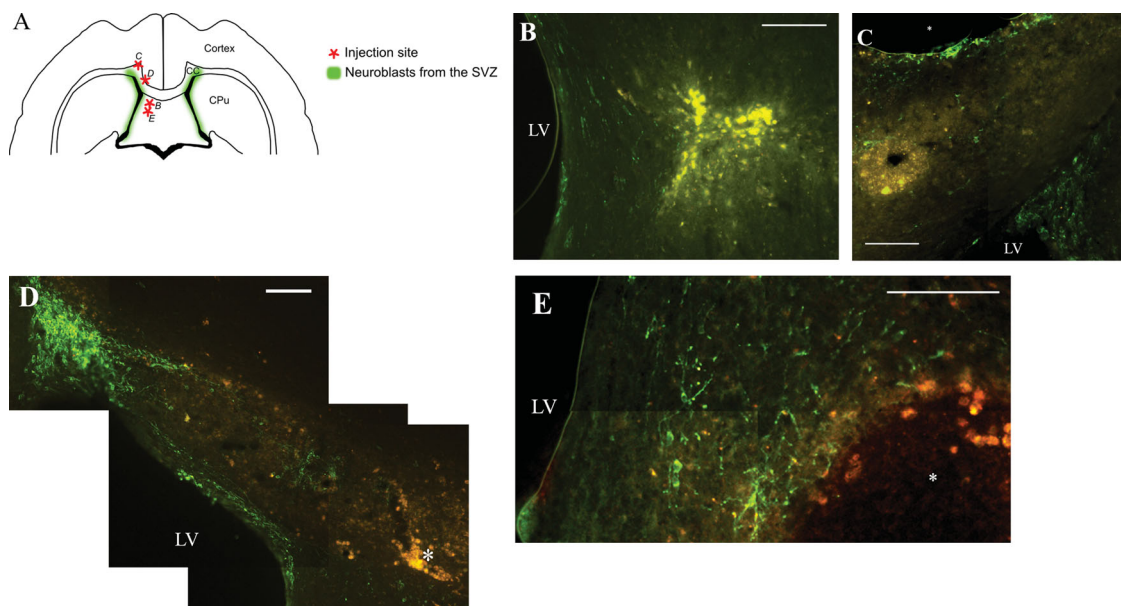


**Figure 5.** A) Schematic illustration of horizontal sections showing the presence of neuroblasts in a layer of tissue surrounding the lateral ventricle (LV), known as the SVZ, and the distribution of neuroblasts near the implant/injury site close to the SVZ. B–E) Horizontal tissue sections immunohistochemically stained for a DCX (green), a marker of neuroblasts. DCX+ cells migrate towards lesion and implants at 7 dpi in response to the needle-induced injury. In lesion only conditions (B), very few DCX+ cells migrated from the SVZ, or located at the lesion boundary. In the case of *Gtn* (not shown in this figure), C) *pGtn*, D) *Gtn+GDNF*, and E) *pGtn+GDNF* implants, there were more DCX+ cell migration from the SVZ, and a greater accumulation of DCX+ at the implant boundary. Yellow color in fluorescent images is autofluorescence from tissue debris at implant/injury site. (\* = implant, scale bar = 100  $\mu\text{m}$ ).

these conjugates tend to phase separate into *Gtn*–HPA-rich components and CMC–Tyr-rich components in solution, and form a porous structure upon crosslinking. In this case, *pGtn* hydrogels exhibited an average pore size of 18–52  $\mu\text{m}$ . The major advantage of phase separation is that it does not require the use of organic solvents or specialized equipment, and is therefore suitable for fabrication of in situ hydrogels. As expected, *pGtn* hydrogel formed from low concentration of HRP (3.9 unit  $\text{L}^{-1}$ ) exhibited the largest pore size. Previous studies<sup>[23]</sup> have shown that decreasing HRP concentration led to an increased gel point (gelation time) of *Gtn* hydrogels. *pGtn* hydrogels formed from lower HRP concentration exhibit larger pores because a longer period of time was available for phase separation to occur prior to gelation.

### 3.2. Attenuation of Reactive Gliosis in the Presence of Hydrogel Porosity

Implantation of *Gtn* resulted in the same GFAP expression profile as injury only. This is characterized by a layer of GFAP+ processes surrounding the injury and a drastic increase in GFAP expression within 200  $\mu\text{m}$  of the injury at 7 dpi; by 21 dpi, GFAP expression in the tissue surrounding the injury returned to normal levels but a glial scar persisted. This indicates that the presence of *Gtn* alone neither exacerbated nor reduced the level of inflammation induced by the injury itself.

The ability of porous structures to attenuate inflammation surrounding an implant and enable cellular infiltration

has been shown in many instances of biomaterial applications.<sup>[36,37]</sup> The optimum pore size for NPC infiltration has not been studied extensively. However, it is generally accepted that the optimum pore size for cell ingrowth ranges from 5 to 300  $\mu\text{m}$ .<sup>[34]</sup> The positive effects that scaffold porosity can have on biocompatibility and tissue integration is well established, and its mechanism is independent of material composition.<sup>[36,38]</sup> The mechanism of action may involve the prevention of glial scar formation. Reactive astrocytes are the prominent cellular component of the glial scar that results in a physical barrier between parenchymal tissue and the implant. An effective barrier requires reactive astrocytes to be in intimate contact with the scaffold surface and form a continuous layer. Pore openings of 18–52  $\mu\text{m}$  within *pGtn* may have acted as obstacles to the formation of a continuous layer of astrocytes. This can allow subsequent infiltration by astrocytes and other cell types,<sup>[39]</sup> although this was not observed in the *Gtn*-based hydrogels. By preventing the buildup of glial cells at the tissue–implant interface, subsequent cellular events are altered, including that of the astrocytes themselves, such that reciprocal interactions between cells and implant become possible. This may not be the only mechanism via which *pGtn* prevented glial scar formation. When pre-formed collagen hydrogels, with average pore size of 100  $\mu\text{m}$ , were implanted into rat brains following a penetrating brain injury, distinct glial scar formation was present at one week, and persisted up to 4 weeks post-implantation.<sup>[10]</sup> However, in such cases, lesion size and intensity of associated inflammatory signals would be a contributing factor to reactive gliosis that is independent of the implanted material.

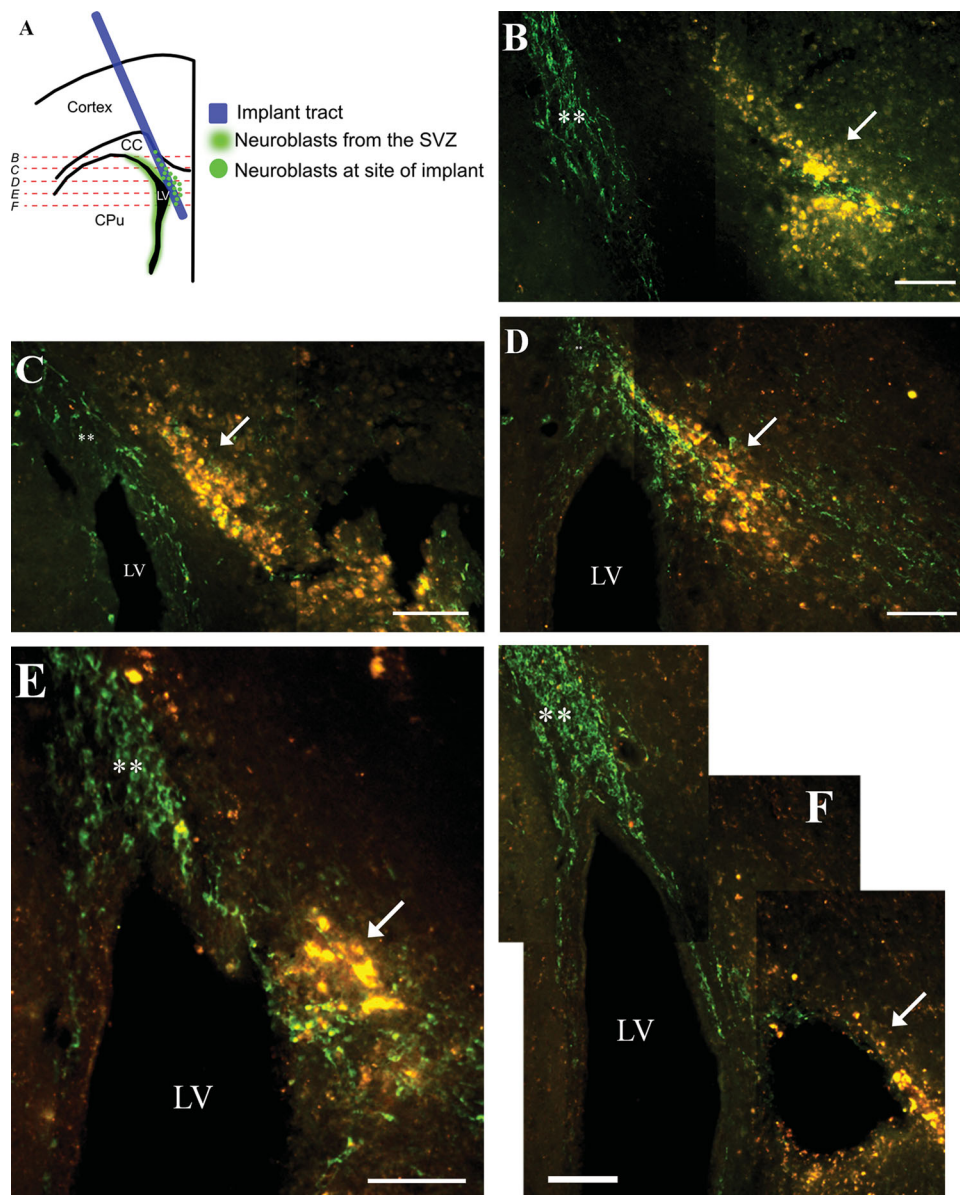


**Figure 6.** Horizontal tissue sections immunohistochemically stained for a DCX (green), a marker of neuroblasts. DCX+ cells originating from the SVZ migrate in the dorsal-ventral direction, along a *Gtn* implant tract, shown schematically in a coronal section (A), and sequential horizontal sections, from dorsal to ventral (B–F). DCX+ cells at the more dorsally located sections (B,C) do not appear to originate from migration within the horizontal plane, due to the lack of DCX+ cells between the anterior SVZ (\*\*\*) and the implant (arrow); DCX+ cells likely originated from more ventral locations of the implant tract (D–F) that intercepted the SVZ. Yellow color in fluorescent images indicate autofluorescence from tissue debris at injury site.

### 3.3. Attenuation of Reactive Gliosis in the Presence of GDNF

Delivery of 0.1 ng of encapsulated GDNF in gelatin-based hydrogels, whether porous or non-porous, significantly reduced the level of GFAP expression surrounding the implant. GDNF is a growth factor that is known to provide trophic support for cells post-injury; administration of exogenous GDNF has been shown to reduce lesion size following ischemia.<sup>[11,40,41]</sup> Hence, it was not surprising that the presence of GDNF reduced the level of reactive gliosis at 7 dpi compared to injury or *Gtn* alone. Of particular significance is that the initial presence of GDNF

was able to almost completely eliminate reactive gliosis by 21 dpi, with no glial scar surrounding the implant, even in the case of non-porous *Gtn*.

#### 3.3.1. GDNF Release Kinetics

There are many reasons to expect that the exogenously delivered GDNF has a very short lifetime within the brain after hydrogel implantation, which can be categorized under two considerations: i) delivery, and ii) clearance from tissue. Delivery of GDNF from the hydrogel is likely to be a diffusion-driven process; due

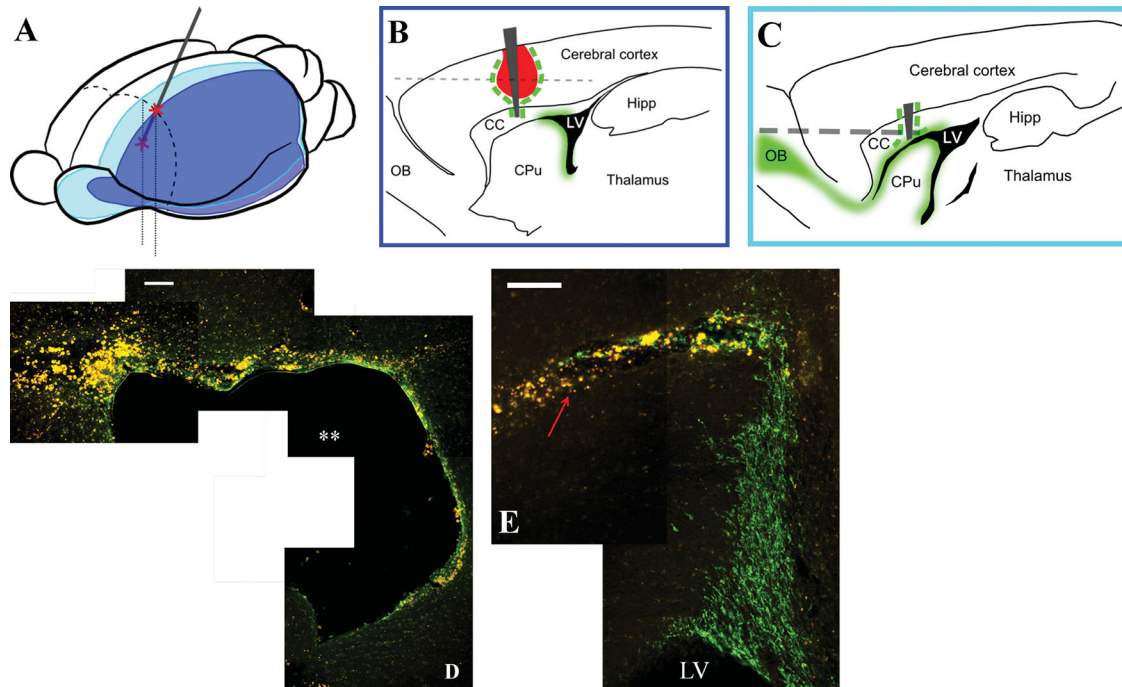


**Figure 7.** Large lesions (>1 mm diameter) induce neuroblast migration towards the injury even at 21 dpi. Needle tract injury is shown schematically in the anterolateral view of the A) whole brain and B) corresponding lateral and C) medial sagittal sections. Dotted lines in B and C indicate location of horizontal sections in D (dorsal) and E (ventral), respectively, showing migration of DCX+ cells from SVZ towards the injury. The large lesion (\*\*\*) was present at the level of the cortex (D), but neuroblasts from more ventral regions of the injury (red arrow, E), where the needle tract disrupted the anterior SVZ (E), clearly migrate towards the injury site. Yellow color in fluorescent images indicates autofluorescence from tissue debris at injury site. [LV = lateral ventricle, Hipp = hippocampus, CC = corpus callosum, CPu = caudate putamen, OB = olfactory bulb. Scale bar = 100  $\mu$ m. B,C) Red = large lesion, gray = needle tract, green = neuroblasts in SVZ and rostral migratory stream, or neuroblasts migrating towards the injury site.]

to the highly porous and hydrated nature of the hydrogel, it can be expected that a large proportion of the GDNF diffuses into the surrounding tissue within hours of implantation. Moreover, since gelation does not occur immediately following implantation, GDNF diffusion from the gelatin solution will be more efficient, leading to a greater initial release if compared to a pre-formed hydrogel. The half-life of GDNF within brain tissue can be relatively short as a result of receptor signaling, which involves endocytosis and retrograde transport.<sup>[42]</sup> When 100  $\mu$ g of GDNF was administered via intracerebroventricular injection, GDNF was able to diffuse through most of the ventricular system with limited superficial penetration into adjacent structures.<sup>[43]</sup> By 7 d post-injection, the majority of the administered GDNF had largely been cleared from the brain tissue, with only small amounts still present in the ventricles. The same study also showed that 24 h after injection into the striatum, GDNF had been distributed to substantia nigra and ventral tegmental area via retrograde transport. The much smaller dose of GDNF (0.1 ng) used in this study was likely to have been cleared away from the tissue much faster. However, since GDNF was encapsulated in the hydrogel, its persistence following implantation would have been longer than if delivered as bolus injection. Within the first week of implantation, the local inflammatory response tends to be at its peak, and it is likely that the GDNF release was further enhanced by partial enzymatic degradation of the hydrogel; therefore, exogenously delivered GDNF is

unlikely to have persisted beyond 7 dpi. Further studies would be required to characterize the kinetics of GDNF release from the Gtn-based hydrogels in vivo.

The unlikely persistence of exogenously delivered GDNF means that it likely exhibited lasting effects on reactive gliosis through its influence on cells at earlier time points when it was still present, thus altering the cascade of subsequent cell signaling events. The short-lived nature of GDNF may explain why no synergism was observed when GDNF delivery was used in combination with the porous hydrogel.

### 3.3.2. Potential Mechanisms

While a reduction in GFAP expression and lack of glial scar formation were associated with the application of GDNF, this effect cannot be attributed to the presence of the delivered GDNF at the time points studied, especially at 21 dpi, since it would have been cleared from the tissue by this stage. A possible explanation for the suppression of reactive gliosis is the ability of GDNF to modulate initial inflammatory events, thus affecting subsequent cellular response, especially that of the reactive astrocytes, which was significantly subdued at 7 dpi. Reactive astrocytes can upregulate expression of various growth factors<sup>[44]</sup>; however, the delayed astrocytic response means that this potential source of neurotrophic factors is absent initially. At early stages of injury, microglial activation

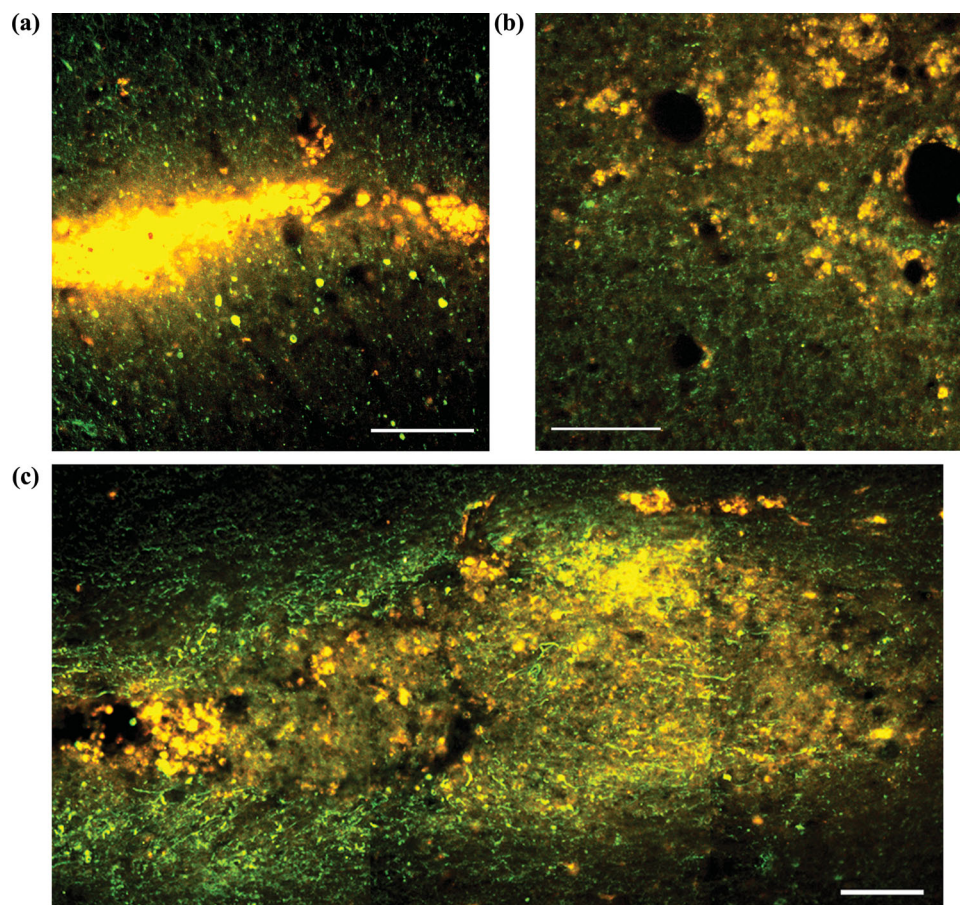


**Figure 8.** Horizontal tissue sections immunohistochemically stained for a SMI32 (green), a marker of sprouting neurites. Presence of SMI32+ cells surrounding A) lesion in injury only, B) *Gtn* only, and C) *pGtn*+*GDNF* implants. No SMI32+ processes infiltrate lesion site (A), but SMI32+ processes do interact and infiltrate to variable degrees into the implanted hydrogel (B and C). Yellow color in fluorescent images indicates autofluorescence from tissue debris at injury site.

will secrete many pro-inflammatory cytokines that mediates the immune response, leading to a cytotoxic environment, and heightened reactive astrogliosis. GDNF-loaded hydrogels provide a local source of GDNF at the implant site that cannot be supplied endogenously at this initial stage of injury. Under *in vitro* conditions, GDNF has been shown to increase the viability of ischemic astrocytes,<sup>[45]</sup> reduce the level of microglial activation, as assessed by the decrease in secretion of inflammatory cytokines, including reactive oxygen species, interleukin 12, and nitric oxide, and reduce phagocytic activity<sup>[46]</sup>; in addition, it can act synergistically with the GSH system in astrocytes to reduce oxidative stress.<sup>[47]</sup> Similarly, *in vivo* delivery of GDNF could have reduced the overall intensity of inflammation and lowered the driving force for glial scar formation either indirectly by reducing cell death, and/or directly by attenuating microglial activation.

The neuroprotective and regenerative effects imparted by GDNF is highly dependent on its method of delivery. Localized and prolonged delivery of GDNF in models of spinal cord injury can have beneficial effects in terms of enhancing astrocyte migration into implant and reduction of glial scar formation at the implant–tissue interface.<sup>[48]</sup> However, prolonged delivery of high doses of GDNF in rat models of stroke failed to

produce neuroprotective effects, and can even exacerbate neuronal damage.<sup>[49]</sup> Variability in the effectiveness of GDNF lies in the different locations of administration, dosages used, and injury model. Effects of GDNF are determined in large by the pattern of GDNF receptors expressed and the degree of upregulation following injury, all of which will vary with specific cell phenotypes and brain regions. The effects of growth factors will also differ greatly with changes in concentrations. In this context, a significant finding of this study is the ability of a relatively small dose of GDNF (0.1 ng, which is at least three orders of magnitude less than other conventionally delivered doses) to drastically reduce inflammation and prevent glial scar formation. Despite the efficacy of such small amounts of GDNF, future applications will benefit from the prolonged, and temporally controlled, delivery of GDNF and/or other growth factors to increase cell infiltration into the hydrogel.

#### 3.4. Neuroblast Migration and Neurite Sprouting

DCX is a microtubule-associated protein that stabilizes microtubules in migrating neuroblasts. It is transiently expressed in immature and migrating neurons typically found in the two

neurogenic niches of the brain—SVZ and SGZ, as well as the RMS. Given the proximity of the implant relative to the SVZ, DCX immunoreactivity was used as a marker of neuroblasts originating from the SVZ.

The pattern of neuroblast distribution at 7 dpi indicates that the injury induced by the needle tract alone is sufficient to induce neuroblast migration towards the lesion. The majority of neuroblast migration appeared to occur along the implant/injury tract (along dorsal–ventral axis), rather than through the parenchymal tissue (along the horizontal plane). This suggests that implants directly intercepting the SVZ can effectively direct neuroblast migration away from the SVZ, and that the implant/lesion boundary represents a path-of-least-resistance for neuroblast migration. The fact that neuroblasts were observed at the lesion boundary only when hydrogels were implanted, but not in injury only animals, suggests that the Gtn-based hydrogels may provide a more permissive environment for the persistence of neuroblasts. At 7 dpi, neuroblasts located outside the SVZ were only present at the implant–tissue interface, with no migrating neuroblasts between the SVZ and the implant, suggesting that the primary tissue damage resulting from the needle tract provided soluble signals to induce neuroblast migration, which cannot be sustained beyond 7 dpi. This may reflect the evolution of the inflammatory response at the lesion and a subsequent reduction in soluble migration-inducing factors. For example, stromal-derived factor-1 $\alpha$  (SDF-1 $\alpha$ ) can induce neuroblast migration via chemotaxis both *in vitro*<sup>[50]</sup> and *in vivo*.<sup>[51,52]</sup> The availability of SDF-1 $\alpha$  depends on the mode and severity of tissue damage. SDF-1 $\alpha$  is actively secreted by various cell types, including reactive astrocytes, activated microglia, and endothelial cells, and can remain elevated for up to 16 weeks post-ischemic damage.<sup>[51,52]</sup> However, in models of TBI, SDF-1 $\alpha$  within the damaged cortex remained elevated for only 3 d, where the increased availability did not result from active cellular synthesis and secretion, but rather due to leakage from the cytoplasm of injured tissue.<sup>[52]</sup> This can explain the short-lived nature of neuroblast migration, as well as the continual neuroblast migration towards relatively large lesions (>1 mm diameter) observed in this study.

A surprising finding in this study was the enhanced presence of neuroblasts at the implant–tissue interface when the implant tract was at the midline of the brain (as implant was crossing from the left hemisphere to the right). Given the relatively long migration distance from the SVZ towards this brain region ( $\approx$ 2.5 mm), this likely reflects an environment that is more conducive to the maintenance of neuroblasts (by promoting cell survival and/or preventing cell maturation) rather than enhanced migration towards this region. Although local differences in microenvironments between brain regions are not surprising, the actual source of difference that would account for this change in neuroblast maintenance is unclear. DCX immunoreactivity is not exclusive to immature neurons, but is also observed in neurons of differentiated morphology under pathological conditions, and even associated with structural plasticity such as sprouting.<sup>[53]</sup> Therefore, enhanced DCX immunoreactivity observed at the midline of the brain may also represent enhanced neuronal plasticity in this brain region. However, this seems unlikely because no enhanced axon regeneration (SMI32

immunoreactivity) was observed. Further studies are required to confirm the cellular identities of DCX+ cells.

Although Gtn-based implants can significantly modify reactive astrogliosis, the presence of reactive astrocytes did not affect the propensity for neuroblast migration. Despite the similarities in GFAP expression between injury and *Gtn* implants, the pattern of neuroblast response and axonal regrowth in *Gtn* implants showed greater similarity with all other implant conditions (which had significantly reduced GFAP expression). Glial scar formation following an injury is important in maintaining a barrier between the damaged and healthy tissues. This is achieved, in part, by the secretion of molecules that are inhibitory to axon regrowth and cell migration. For example, expression of chondroitin sulfate proteoglycans is increased within the glial scar following CNS injuries, and reactive astrocytes are a major source of these inhibitory molecules.<sup>[54]</sup> This is apparent in the injury condition, where no axonal regrowth was observed extending into the lesion core. In contrast, axonal regrowth can extend beyond the lesion boundary for all implanted materials, including the *Gtn* implants, where astrogliosis was heightened. This indicates that *Gtn*-based implants can modify the behavior of reactive astrocytes, such that the local microenvironment is less inhibitory to axonal regrowth. Moreover, given the propensity for neuroblasts to migrate dorsally along the implant/lesion interface, the glial scar does not seem to exert inhibitory influences on neuroblast migration or maintenance.

The absence of DCX+ staining at 21 dpi suggests that the neuroblasts were either not viable or had undergone differentiation into mature phenotypes. The possibility of neuronal differentiation and non-viability is consistent with previous studies of stroke-induced neuroblast migration, where DCX+ cells at the lesion site have already differentiated into mature phenotypes, as indicated by expression of NeuN, albeit only a small proportion of the initial DCX+ cohort remained viable.<sup>[8]</sup> The process of neuroblast migration from SVZ to OB, and subsequent differentiation at the OB typically takes 7 d.<sup>[55]</sup> Therefore, it is highly plausible that some of the DCX+ cells observed in this study had undergone neuronal differentiation between 7 and 21 dpi; however, their survival and functional integration remain to be determined.

Incorporation of GDNF into the hydrogels not only significantly reduced inflammation, but it also increased both axon regeneration and neuroblasts at the implant boundary. It is possible that this is a direct consequence of GDNF released into the surrounding tissue and exerting trophic effects on surviving neurons and undifferentiated neuroblasts. However, as previously mentioned, the exogenously delivered GDNF is unlikely to persist at 7 dpi, and improvements in axon regeneration may be attributed to the modulation of the inflammatory response, which perhaps dampened the cytotoxic effects and promoted a trophic response. The absence of extensive NPC and neurite sprouting that penetrate deep into the hydrogel may be a reflection of the collapse of the porous microstructure with time, or the general low affinity of neural cells for collagen- and gelatin-based hydrogels.<sup>[10,21]</sup> Rapid diffusion of GDNF out of the hydrogel may deplete the implant itself of trophic factors, which may be critical for attracting neuroblasts and regenerating axons into the material.

The essential factors required for the continued survival of NPCs at the site of injury are not fully elucidated, but it is apparent that temporal control of growth factor release from an implant is as important as the type and dosage, and future hydrogel modifications should take this into account.

#### 4. Conclusions

This study shows that the introduction of porosity or low-dose GDNF can effectively attenuate the reactive astroglial response and improve the interaction between the implant and surrounding tissue. However, it is unclear whether *pGtn* or the delivered GDNF attenuated reactive astrogliosis by acting directly on astrocytes, or indirectly by affecting other cell types that are more prominent immediately following injury, which subsequently altered astrocyte behavior, or a combination of the two.

When hydrogel implants disrupted the SVZ, some neuroblasts can be actively diverted to migrate towards and dorsally along the implant tract at 7 dpi. Neuroblasts were only rarely observed at the lesion boundary (in the absence of implants), indicating that the *Gtn*-based hydrogels provided an environment that fostered the maintenance and/or survival of these neuroblasts. Increased neuroblast migration was associated with GDNF-incorporated hydrogel implants; however, this effect did not persist at 21 dpi. No neuroblast migration was observed at 21 dpi for all implant conditions, indicating that in the absence of additional signaling, long-term neuroblast migration cannot be sustained in this injury model. The fate of these neuroblasts at the implant/lesion boundary was not determined, but the lack of cellular infiltration into the implants suggests that these cells may not have survived in the long-term for neural regeneration.

#### 5. Experimental Section

**Hydrogel Formation:** The preparation of the porous gelatin (*pGtn*) hydrogel was carried out according to a previously developed procedure.<sup>[27]</sup> In brief, *Gtn* was functionalized with HPA to form gelatin-HPA (*Gtn*-HPA) conjugates, and CMC with Tyr to form CMC-Tyr conjugates, using a carbodiimide/active ester-mediated coupling reaction. Conjugation reactions were confirmed by <sup>1</sup>H NMR (D<sub>2</sub>O). Non-porous *Gtn*-HPA (*Gtn*) hydrogels were prepared with *Gtn*-HPA (2 wt%), H<sub>2</sub>O<sub>2</sub> (1.7 × 10<sup>-3</sup> M), and HRP (6.25 units L<sup>-1</sup>; Novachem Pty Ltd.). Crosslinking occurred via enzymatic oxidative coupling of phenol moieties in HPA, in the presence hydrogen peroxide (H<sub>2</sub>O<sub>2</sub>, acting as an oxidant) and catalyzed by HRP. Porous gelatin-based *pGtn* hydrogels were prepared with a polymer mixture (5 wt%) consisting *Gtn*-HPA and CMC-Tyr (in the ratio 80:20, w/w), H<sub>2</sub>O<sub>2</sub> (1.7 mM), and HRP (3.9 units L<sup>-1</sup>). In this case, hydrogel formation occurred as a result of the same coupling mechanism between phenol groups on HPA and/or Tyr residues to form crosslinks between polymer chains. Differential hydrophobicity between *Gtn*-HPA and CMC-Tyr led to phase separation during gel formation, and was the basis for pore formation.<sup>[27]</sup> For GDNF-blended hydrogels, GDNF (100 ng mL<sup>-1</sup>; recombinant human GDNF, R&D Systems) was incorporated into the polymer solution prior to gelation. For an injection volume of approximately 1.2–1.5 μL, this corresponds to a GDNF load of approximately 0.1 ng per injection.

**Hydrogel Characterization:** The swell ratio of *pGtn* was measured by using hydrogel disks, formed with H<sub>2</sub>O<sub>2</sub> (49.8 × 10<sup>-6</sup> M), HRP (3.9, 7.7,

and 15.5 units L<sup>-1</sup>), and immersed in PBS at 37 °C for 2 d to reach swelling equilibrium. The swollen disks were gently blotted dry on the surface and weighed to measure the wet weight (*M*<sub>wet</sub>). The disks were then lyophilized and weighed to obtain the dry weight (*M*<sub>dry</sub>). The swelling ratio (SR) was determined according to Equation (1),

$$SR = \frac{M_{wet} - M_{dry}}{M_{dry}} \quad (1)$$

The porous structure of lyophilized *pGtn* was examined by SEM. The porous structure of hydrated *pGtn* was examined by confocal microscopy. For visualization in confocal microscopy, the hydrogels were prepared using fluorescently labeled *Gtn*-HPA. To synthesize fluorescently labeled *Gtn*-HPA, the carboxyl group of *Gtn*-HPA (10 g) was activated by 1-ethyl-3-(3-dimethylaminopropyl)-carbodiimide hydrochloride (0.3 × 10<sup>-6</sup> M; Sigma-Aldrich) and *N*-hydroxysuccinimide (0.3 × 10<sup>-6</sup> M; Sigma-Aldrich) at pH 4.8 for 15 min. Fluoresceinamine isomer I (0.23 × 10<sup>-6</sup> M; Sigma-Aldrich) in methanol (2 mL) was then added dropwise to the activated *Gtn*-HPA while stirring. The reagents were allowed to react overnight in the dark. The product was dialyzed against milliQ water for 3 d prior to lyophilization. The pore size and porosity of the lyophilized scaffold were measured using a mercury porosimeter (Autopore II 9220, Micromeritics Co.).

**In Vivo Implantation:** All animal procedures were approved by the Howard Florey Institute Ethics committee (#10-017) and in accordance with the National Health and Medical Research Council guidelines. Male Wistar rats (≈300 g, *n* = 40) were used for implantation studies. Anesthesia was induced with an intramuscular injection of atropine (0.1 mL) and xylazine (0.2 mL; Troy Laboratories Pty Ltd.) in saline, followed by inhalation of isoflurane gas (3% administered at 1.5 L/min). Rats were mounted onto a stereotaxic frame where the delivery of anesthesia continued via a nose-cone. Hot-water bottles and heat pads were used to maintain the rat's body temperature during surgery and post-operative recovery. The skull was revealed by cutting and exposing the skin along the midline of the scalp. To assess the ability of the hydrogel to influence stem cell migration, there were two separate injections to target the SVZ in the two hemispheres. Due to limitations of equipment setup, we approached both lateral ventricles (LVs) from the left hemisphere; the two injection sites are termed the lateral site (targeting the ipsilateral LV), and the medial site (targeting the contralateral LV). A small piece of skull bone was removed with a dental drill at the following positions: 1.0 mm anterior of bregma, 1.3 mm (medial site) and 3.0 mm (lateral site) lateral to the midline in the left hemisphere. The hydrogel solution was pre-loaded into a 21G needle and injected into the brain at an angle of 25° from the vertical in the coronal plane. The hydrogel inserted via the medial site had an injection length of 7 mm, which passed through the LV and terminated in the caudate putamen of the right hemisphere. When inserted via the lateral site, the injection length was 6 mm, which passed through the caudate putamen and LV, and terminated in the ventral part of the lateral septal nucleus (LSV) in the left hemisphere. Rats were bilaterally implanted with *Gtn* hydrogel, *pGtn* hydrogel, *Gtn* hydrogel loaded with GDNF (100 ng mL<sup>-1</sup>; *Gtn*+GDNF), or *pGtn* hydrogel loaded with GDNF (100 ng mL<sup>-1</sup>; *pGtn*+GDNF). As a control, surgery was performed as previously described to create an equivalent injury, but no hydrogels were implanted (injury). Eight rats were randomly allocated to each treatment group, with half the rats in each treatment group (*n* = 4) sacrificed at each of the designated time points (7 and 21 d).

The rats were sacrificed at 7 and 21 dpi with sodium pentobarbitone (0.125 mL; Letha-barb) and heparin (0.54 mg, 188 USP units mg<sup>-1</sup>; Sigma-Aldrich), followed by perfusion with PBS (250 mL, 0.2 M) and then paraformaldehyde (PFA) (300 mL, 4%; Sigma-Aldrich) at 4 °C. Brains were removed and post-fixed for 24 h in PFA (4%), after which it was soaked in sucrose solution (30% in PBS) for 2 d. All brains were frozen in liquid nitrogen and stored at -80 °C. Horizontal sections of 30-μm thickness were obtained using a cryostat (Leica) in preparation for immunocytochemistry.

**Immunocytochemistry:** Brain sections were fixed in PFA (4%) for 2 min then washed in PBS (3 × 5 min). A blocking solution containing normal goat serum (3%) and Triton-X (0.3%) was applied for 1 h at

room temperature. The sections were incubated in the following primary antibodies overnight at 4 °C: mouse anti-GFAP Cy3-conjugated (1:400; Sigma–Aldrich), rabbit DCX polyclonal antibody (1:300; Cell Signaling Technology), and mouse anti-neurofilament (SMI32) monoclonal antibody (1:1000; Covance). All sections were washed in PBS (3 × 5 min). Sections stained with DCX and SMI32 were incubated in a secondary antibody of anti-rabbit and anti-mouse AlexaFluor488 (1:1000; Molecular Probes), respectively, for 2 h at room temperature. These sections were washed in PBS (3 × 5 min). All slides were mounted in Dapi (VectorShield and coverslipped. GFAP, DCX, and SMI32 are markers of astrocytes, migrating neuroblasts, and sprouting of neurites and dendrites, respectively. Brain sections were imaged using a fluorescence microscope (Leica LM2500).

**Statistical Analysis:** Astrogliosis was quantified by measuring the average GFAP fluorescence intensity over rectangular areas (100 μm thick) at 200 μm intervals from the implant/lesion boundary. Average GFAP fluorescence intensity over the 100 μm × 200 μm rectangular area was determined by measuring the average gray-scale pixel intensity using ImageJ, and expressed relative to an uninjured area of corresponding brain regions on the same section. Results were expressed as mean ± standard error, and one-way ANOVA with Tukey's post hoc testing was performed (GraphPad InStat Version 3.10);  $p < 0.05$  was used for determining statistical significance.

## Supporting Information

Supporting Information is available from the Wiley Online Library or from the author.

## Acknowledgements

Funding for this work was partly provided through Australian Research Council Discovery Project Grants DP120102570 and DP0985433. P.J.C. is supported by the ARC Future Fellowship scheme. This work was performed in part at the Melbourne Centre for Nanofabrication. P.P.Y.C. is grateful for an MCN Technology Fellowship that supported this work, and a RMIT University Senior Research Fellowship.

Received: July 16, 2013

Revised: October 11, 2013

Published online: March 4, 2014

- [1] K. Hernandez-Ortega, R. Quiroz-Baez, C. Arias, *Neurosci. Bull.* **2011**, 27, 185.
- [2] H. K. Eltzschig, T. Eckle, *Nat. Med.* **2011**, 17, 1391.
- [3] D. Shlosberg, M. Benifla, D. Kaufer, A. Friedman, *Nat. Rev. Neurol.* **2010**, 6, 393.
- [4] D. J. Loane, A. I. Faden, *Trends Pharmacol. Sci.* **2010**, 31, 596.
- [5] J. V. Rosenfeld, A. I. Maas, P. Bragge, M. C. Morganti-Kossmann, G. T. Manley, R. L. Gruen, *Lancet* **2012**, 380, 1088.
- [6] A. Heile, T. Brinker, *Dialogues Clin. Neurosci.* **2011**, 13, 279.
- [7] J. J. Cunningham, T. M. Ulbright, M. F. Pera, L. H. J. Looijenga, *Nat. Biotechnol.* **2012**, 30, 849.
- [8] A. Arvidsson, T. Collin, D. Kirik, Z. Kokaia, O. Lindvall, *Nat. Med.* **2002**, 8, 963.
- [9] J. M. Parent, Z. S. Vexler, C. Gong, N. Derugin, D. M. Ferriero, *Ann. Neurol.* **2002**, 52, 802.
- [10] P. Z. Elias, M. Spector, *J. Neurotrauma* **2012**, 29, 2086.
- [11] E. P. Duarte, M. Curcio, L. M. Canzoniero, C. B. Duarte, *Growth Factors* **2012**, 30, 242.
- [12] T. Alexi, C. V. Borlongan, R. L. M. Faull, C. E. Williams, R. G. Clark, P. D. Gluckman, P. E. Hughes, *Prog. Neurobiol.* **2000**, 60, 409.
- [13] C. Consales, F. Volpicelli, D. Greco, L. Leone, L. Colucci-D'Amato, C. Perrone-Capano, U. di Porzio, *Brain Res.* **2007**, 1159, 28.
- [14] S. S. Gill, N. K. Patel, G. R. Hottot, K. O'Sullivan, R. McCarter, M. Bunnage, D. J. Brooks, C. N. Svendsen, P. Heywood, *Nat. Med.* **2003**, 9, 589.
- [15] Z. Zhao, S. Alam, R. W. Oppenheim, D. M. Prevette, A. Evenson, A. Parsadianian, *Exp. Neurol.* **2004**, 190, 356.
- [16] S. Gorgieva, V. Kokol, in *Biomaterials Applications for Nanomedicine*, (Ed: R. Pignatello), InTech, Rijeka, Croatia **2011**.
- [17] D. Bonneh-Barkay, C. A. Wiley, *Brain Pathol.* **2009**, 19, 573.
- [18] H. M. Powell, S. T. Boyce, *Tissue Eng. Part A* **2009**, 15, 2177.
- [19] K. Cheng, A. Blusztajn, D. Shen, T.-S. Li, B. Sun, G. Galang, T. I. Zarebinski, G. D. Prestwich, E. Marbán, R. R. Smith, L. Marbán, *Biomaterials* **2012**, 33, 5317.
- [20] L. Ghasemi-Mobarakeh, M. P. Prabhakaran, M. Morshed, M.-H. Nasr-Esfahani, S. Ramakrishna, *Biomaterials* **2008**, 29, 4532.
- [21] K. Deguchi, K. Tsuru, T. Hayashi, M. Takaishi, M. Nagahara, S. Nagotani, Y. Sehara, G. Jin, H. Zhang, S. Hayakawa, M. Shoji, M. Miyazaki, A. Osaka, N.-H. Huh, K. Abe, *J. Cereb. Blood Flow Metab.* **2006**, 26, 1263.
- [22] K.-F. Huang, W.-C. Hsu, W.-T. Chiu, J.-Y. Wang, *Biomaterials* **2012**, 33, 2067.
- [23] L.-S. Wang, J. E. Chung, P. P. Y. Chan, M. Kurisawa, *Biomaterials* **2010**, 31, 1148.
- [24] T. C. Lim, W. S. Toh, L.-S. Wang, M. Kurisawa, M. Spector, *Biomaterials* **2012**, 33, 3446.
- [25] W. S. Toh, T. C. Lim, M. Kurisawa, M. Spector, *Biomaterials* **2012**, 33, 3835.
- [26] L.-S. Wang, J. Boulaire, P. P. Y. Chan, J. E. Chung, M. Kurisawa, *Biomaterials* **2010**, 31, 8608.
- [27] A. Al-Aboodi, J. Fu, P. M. Doran, P. P. Y. Chan, *Biotechnol. Bioeng.* **2013**, 110, 318.
- [28] D. R. Nisbet, A. E. Rodda, M. K. Horne, J. S. Forsythe, D. I. Finkelstein, *Tissue Eng. Part A* **2010**, 16, 2833.
- [29] C.-Y. Yang, B. Song, Y. Ao, A. P. Nowak, R. B. Abelowitz, R. A. Korsak, L. A. Havton, T. J. Deming, M. V. Sofroniew, *Biomaterials* **2009**, 30, 2881.
- [30] M. V. Sofroniew, *Neuroscientist* **2005**, 11, 400.
- [31] D. W. Hampton, K. E. Rhodes, C. Zhao, R. J. M. Franklin, J. W. Fawcett, *Neuroscience* **2004**, 127, 813.
- [32] F. Lee, J. E. Chung, M. Kurisawa, *J. Controlled Release* **2009**, 134, 186.
- [33] F. J. O'Brien, B. A. Harley, I. V. Yannas, L. J. Gibson, *Biomaterials* **2005**, 26, 433.
- [34] S. H. Oh, I. K. Park, J. M. Kim, J. H. Lee, *Biomaterials* **2007**, 28, 1664.
- [35] S. J. Bryant, J. L. Cuy, K. D. Hauch, B. D. Ratner, *Biomaterials* **2007**, 28, 2978.
- [36] D. Y. Wong, P. H. Krebsbach, S. J. Hollister, *J. Neurosurg.* **2008**, 109, 715.
- [37] B. D. Ratner, *Polym. Int.* **2007**, 56, 1183.
- [38] F. Bai, J. Zhang, Z. Wang, J. Lu, J. Chang, J. Liu, G. Meng, X. Dong, *Biomed. Mater.* **2011**, 6, 015007.
- [39] D. A. Kristt, *J. Neuropathol. Exp. Neurol.* **1987**, 46, 668.
- [40] W. Wang, C. Redecker, H.-J. r. Bidmon, O. W. Witte, *Brain Res.* **2004**, 1023, 92.
- [41] W. R. Zhang, T. Hayashi, M. Iwai, I. Nagano, K. Sato, Y. Manabe, K. Abe, *Brain Res.* **2001**, 903, 253.
- [42] A. Tomac, J. Widenfalk, L. F. Lin, T. Kohno, T. Ebendal, B. J. Hoffer, L. Olson, *Proc. Natl. Acad. Sci.* **1995**, 92, 8274.
- [43] P. A. Lapchak, S. Jiao, F. Collins, P. J. Miller, *Brain Res.* **1997**, 747, 92.
- [44] E. Appel, O. Kolman, G. Kazimirsky, P. M. Blumberg, C. Brodie, *Neuroreport* **1997**, 8, 3309.

- [45] C.-H. Lin, F.-C. Cheng, Y.-Z. Lu, L.-F. Chu, C.-H. Wang, C.-M. Hsueh, *Exp. Neurol.* **2006**, *201*, 225.
- [46] S. M. Rocha, A. C. Cristovão, F. L. Campos, C. P. Fonseca, G. a. Baltazar, *Neurobiol. Dis.* **2012**, *47*, 407.
- [47] J. K. Sandhu, M. Gardaneh, R. Iwasiow, P. Lanthier, S. Gangaraju, M. Ribecco-Lutkiewicz, R. Tremblay, K. Kiuchi, M. Sikorska, *Neurobiol. Dis.* **2009**, *33*, 405.
- [48] L.-X. Deng, J. Hu, N. Liu, X. Wang, G. M. Smith, X. Wen, X.-M. Xu, *Exp. Neurol.* **2011**, *229*, 238.
- [49] A. Arvidsson, D. Kirik, C. Lundberg, R. J. Mandel, G. Andsberg, Z. Kokaia, O. Lindvall, *Neurobiol. Dis.* **2003**, *14*, 542.
- [50] J. Imitola, K. Raddassi, K. I. Park, F.-J. Mueller, M. Nieto, Y. D. Teng, D. Frenkel, J. Li, R. L. Sidman, C. A. Walsh, E. Y. Snyder, S. J. Khoury, *Proc. Natl. Acad. Sci.* **2004**, *101*, 18117.
- [51] P. Thored, A. Arvidsson, E. Cacci, H. Ahlenius, T. Kallur, V. Darsalia, C. T. Ekdahl, Z. Kokaia, O. Lindvall, *Stem Cells* **2006**, *24*, 739.
- [52] T. Itoh, T. Satou, H. Ishida, S. Nishida, M. Tsubaki, S. Hashimoto, H. Ito, *Neurol. Res.* **2009**, *31*, 90.
- [53] J. Nacher, C. Crespo, B. S. McEwen, *Eur. J. Neurosci.* **2001**, *14*, 629.
- [54] R. McKeon, R. Schreiber, J. Rudge, J. Silver, *J. Neurosci.* **1991**, *11*, 3398.
- [55] J. P. Brown, S. Couillard-Després, C. M. Cooper-Kuhn, J. Winkler, L. Aigner, H. G. Kuhn, *J. Comp. Neurol.* **2003**, *467*, 1.